SUPPLEMENTARY METHODS

Mice, tumors, irradiation and tissue preparation: C57BL/6J (Stock #000664), sv129/BL6 (Stock #101045) male mice, C3H/HeJ ($MMTV^-$) male mice (Stock #000659), and B6.CB17-Prkdcscid/SzJ (SCID) male mice (Stock # 001913), 8-12 weeks old, were purchased from The Jackson Laboratory (Bar Harbor, ME). C57BL/$6^{asmase-/-}$, SV129/C57BL/$6^{asmase-/-}$ and $SCID^{asmase-/-}$ mice were bred as described (1). Construction of *asmase*$^{-/-}$ mice: the PGK-neomycin expression cassette was inserted into exon 2 of the murine *asmase* genomic sequence, disrupting the coding sequence and facilitating positive selection of gene targeting events (2). Genotyping used a modification of the protocol described (2), employing a revised PA2 primer (5′-GGCTACCCGTGATATTGC-3′), and 35 cycles of PCR amplification, each at 94°C for 15 sec, 64°C for 30 sec, and 68°C for 90 sec.

Mouse B16F1 melanoma (3), MCA/129 fibrosarcoma (4), and human HCT116 colorectal carcinoma (ATCC) cells were cultured in Dulbecco's modified essential medium (DMEM) high glucose, 10% fetal bovine serum, and 100 U/ml penicillin and 100 µg/ml streptomycin. To produce tumors, $1x10^6$ cells in 100-230µl PBS were injected into the lateral abdominal subcutaneous tissue as described (1). Mouse mammary MCa tumor cells (5) were maintained and transplanted as previously described (6). Briefly, a single tumor cell suspension was prepared from solid tumor by removing necrotic tissue and disaggregating tumor using a glass pestle on a stainless steel mesh immersed in phosphate-buffered saline containing Ca^{2+} and Mg^{2+} followed by repeated aspiration through a 22 gauge needle. $1x10^6$ cells in 100 µl PBS were injected into the right subcutaneous foot of syngeneic C3H/HeJ ($MMTV^-$) mice.

Cell lines were irradiated using cesium Shepard irradiator (1.6Gy/min). Tumors were irradiated at a size of 100-150 mm^3 as described (1) using a Pantak Siefert Systems X-ray 320 machine (1.17Gy/min). A cylindrical lead jig was devised to allow exposure of tumor only. Ketamine (0.1 mg/kg) and xylazine (0.02 mg/g) sedation were used. Tumor volume was monitored using a sliding jaw caliper and quantified a hemi-ellipsoid approximation $V=\pi/6$ abc with a, b, c denoting the 3 perpendicular diameters (7).

BQ-123 (2 mg/kg; Sigma-Aldrich B150-200UG) was administrated by intraperitoneal injection at 30 min prior to SDRT. 4-Hydroxy-2,2,6,6-tetramethylpiperidine1-oxyl (Tempol, 300 mg/kg, Sigma-Aldrich #176141) was administrated by intraperitoneal injection at 30 min after SDRT in WT mice or immediately after clamp release in *asmase*$^{-/-}$ mice. When indicated, tumor specimens were fixed in 4% fresh formaldehyde, embedded in paraffin, and 3- or 5µm-sections were stained as described(1).

TUNEL, MECA-32 double staining of apoptotic nuclei: Tumor specimens were obtained after SDRT, fixed in 4% fresh formaldehyde, embedded in paraffin, and 5mm-sections were evaluated for apoptosis by terminal deoxytransferase-mediated deoxyuridine triphosphate nick end labeling (TUNEL) (Roche #3333574001 #11093070910), as described (8). Endothelial cells were identified in TUNEL stained sections using an antibody specific for the pan-endothelial cell marker MECA-32 (1). Briefly, TUNEL stained sections were incubated with the anti- MECA-32 mouse monoclonal antibody (1:10 dilution; DSHB), and staining was developed using biotinylated anti-rat antibodies (1:100 dilution; Vector Laboratories), the avidin-biotin

peroxidase complex (Vector Laboratories) and True Blue Peroxidase substrate as final chromogen (KPL Laboratories). Apoptotic endothelial cells in tumor tissue were identified microscopically as displaying a brown TUNEL-positive nuclear signal surrounded by dark-blue plasma membrane signal indicative of MECA-32 staining.

Quantification of SUMO2/3 in whole tumor lysates and in cytosolic and chromatin-enriched sub-fractions: Whole tumor cell extracts from fresh or fresh frozen specimens were generated as described (9). Briefly, frozen tumors were ground with a rotor homogenizer in lysis buffer containing 50mM β-glycerophosphate, 1mM EDTA, 1mM EGTA, 0.5mM Na_3VO_4, 1% Triton X-100 and 2% SDS supplemented with Protease Inhibitor Cocktail (Sigma-Aldrich #11836170001), 20mM N-ethylmaleimide and iodoacetamide (Sigma-Aldrich #E3876). Lysates were immediately boiled at 99˚C for 5 min and then centrifuged at 14,000g for 10 min at 4˚C.

For fractionation of whole extracts into cytoplasmic and chromatin-enriched fractions was performed as per (10). Briefly, frozen tumors were processed using Dounce homogenizers in buffer #1 containing 10mM HEPES (4-(2-hydroxyethyl)-1-piperazineethanesulfonic acid), 10mM KCl, 1.5mM $MgCl_2$, 0.34M sucrose, 10% glycerol and 1mM dithiothreitol (DTT) supplemented with Protease Inhibitor Cocktail, 20mM N-ethylmaleimide and iodoacetamide. 0.1% Triton X-100 was added and homogenates were incubated for 5 min on ice. Nuclei were pelleted by centrifugation at 1300g for 4 min at 4°C. The supernatant was considered the cytoplasmic fraction. The pellet was washed once in buffer #1 and then lysed in buffer #2 containing 3mM EDTA, 0.2mM EGTA and 1mM DTT supplemented with Protease Inhibitor Cocktail (Sigma-Aldrich #11836170001), 20mM N-ethylmaleimide and iodoacetamide. Insoluble chromatin was collected by centrifugation at 1700g for 4 min at 4°C and washed once in buffer #2. The final chromatin pellet was resuspended in Laemmli Buffer supplemented with 20mM N-ethylmaleimide and iodoacetamide and sonicated in a Misonix Ultrasonic processor XL2020 sonicator for 15sec using a microtip at 20% amplitude.

For evaluation of free SUMO2/3 or SUMO2/3-conjugated protein complexes, Western blotting (WB) analysis was employed. After protein concentration was measured using Biorad DC protein assay (Biorad #500-0114), samples were boiled for 5 min in sample buffer without β-mercaptoethanol, and subjected (15-50 μg/ lane) to SDS-PAGE (6-15%) separation and transferred onto Immuno-Blot PVDF (polyvinylidene fluoride) membrane (Biorad #1620177). WB was performed using either rabbit polyclonal anti-SUMO2/3 (Abcam #ab3742, dilution 1:2000), mouse monoclonal anti-SUMO2/3 (MBL [clone1E7], #M114-3, dilution 1:2000), rabbit polyclonal anti-histone H3 (Abcam #ab1791, dilution 1:10000), mouse monoclonal anti-tubulin (Abcam [clone DM1A], #ab7291, dilution 1:5000) or rabbit polyclonal anti-β-actin (Biolegend #622102, dilution 1:2000) antibodies. Anti-mouse HRP (GE Healthcare #NA931, dilution 1:10,000) and anti- rabbit HRP (GE Healthcare #NA934, dilution 1:20,000) were used for secondary Ab detection. The detection signal was developed using WB Detection Reagent (Amersham ECL #RPN2106) or Immobilon Western Chemiluminescent HRP substrate (Millipore #WBKLS0500) and exposed to Hyperfilm ECL (Amersham #29806839). Densitometric analysis was carried out using Image J software (NIH, https://imagej.nih.gov/ij/).

RNA isolation and cDNA synthesis*:* Total RNA was extracted from cells at passage 2 and at passage 4-5 using RNeasy Mini Kit following manufacturer's instructions (Qiagen #74104). Total RNA was extracted from tumors conserved in RNAlater using RNeasy Mini Kit following manufacturer's instructions (Qiagen). Complementary DNA (cDNA) was synthesized from total RNA using the Superscript III First-strand system Kit (Invitrogen #18080051).

Generation of the shRNA lines shSUMO2, shSUMO3: ShSUMO-2 (V3LHS-386696, V3LHS-412780), ShSUMO-3 (V3LHS-326172, V3LHS-403521) GIPZ lentiviral particles from GE Dharmacon were used to transduce HCT116 cells following manufacturer's instruction. ShScramble was used as a non-silencing shRNA control (#RHS4348). Transduced cells, selected in media containing 2 µg/ml puromycin were maintained in 1 mg/ml puromycin and used for experiments during passage 2-5.

SUMO2 and SUMO3 gene expression: Gene expression for *SUMO2* (#Hs02743873_g1), *SUMO3* (#Hs00739248_m1) and *TP53BP1* (#Hs00996818_m1) was measured using TaqMan Gene Expression Assay primers (Applied Biosystems) and Master Mix (Applied Biosystems, #4304437) using an Applied Biosystems 96-well Thermal Cycler. *TBP* (#4332659) and *GUSB* (#4332655) were used to normalize gene expression levels.

Generation of the PRDX6 overexpression: Myc-tag Peroxiredoxin-6 (Prdx6) vector (MG51391-NM Sino Biological), or a negative control vector (CV017 Sino Biological) was used to transfect MCA/129 fibrosarcomas employing lipofectamine 3000. Transfected cells were selected using 200 µg/ml hygromycin (10687010 ThermoFisher scientific) for 14 days, trypsinized, washed 3 times with PBS and part of cells pellet was used to determine Myc-tag Prdx6 overexpression on cells extract western blot. Another portion of the pellet was suspended in PBS and injected ($1x10^6$ cells) into the subcateneous flank tissue of sv129/BL6 mice to generate tumors for experiment.

Proliferation assay: Cells were quantified by hemocytometer, using trypan blue exclusion to assure viability. $2x10^5$ cells were plated in triplicate in Dulbecco's modified essential medium (DMEM) high glucose, 10% fetal bovine serum, and 100 U/ml penicillin and 100 µg/ml streptomycin, and 24h later irradiated with 5Gy. Cell quantification was performed daily using a Reichert Hemocytometer for 6 days.

Dihydroethidium (DHE) staining: Staining was done according to the Emory University, School of Medicine (Atlanta, GA) protocol with minor modifications. Briefly, at 1h post SDRT, tumors were harvested, rinsed immediately in cold (4°C) PBS, placed in Tissue-Tek optimal cutting temperature compound (OCT, Electron Microscopy Sciences, #62550-01), and snap frozen in dry ice isopentane slurry. Within 2-4h after harvest, 3 µm-thick cryosections of unfixed frozen segments were cut using a Leica CM1950 cryostat and placed on a glass slide. DHE, suspended in DMSO at stock concentrations of 10mM, was diluted to a final concentration of 1µM in PBS. Slides were incubated in a light-protected humidified incubator at 37°C for 30 min, counterstained with 4',6-diamidino-2-phenylindole dihydrochloride (DAPI) and mounted in Mowiol Mounting

Medium. Sections were examined at 30 min after staining and within 5-7h of harvest with a Leica-Upright Confocal Microscope at 40X magnification (fluorescence of ethidium Ex:Em=510/595 nm). Quantification was done using an automated program for Fiji software (NIH) calculating the DHE-positive area within the DAPI-positive area.

Micronucleus assay: Micronuclei (MN) in vivo were detected histologically in 3μm H&E-stained tumor sections after 15Gy SDRT in mononucleate or binucleate cells as described(11). MN were also determined ex vivo using the cytochalasin B cytokinesis-block method, as described(12). Tumors were irradiated in vivo and 30 min later excised, minced, and incubated for 30 min at 37°C in buffer containing 166 U/ml collagenase XI (Sigma #C7657), 0.25 mg/ml *S. griseus* protease (Sigma #P5147) and 255 U/ml DNAase (Sigma #D4527) in HEPES-buffered saline solution (HBSS) solution. Dissociated cells in 3X volume of 15% FCS-DMEM medium were strained through a 70mm mesh, and centrifuged at 500xg. Pelleted cells were re-suspended in culture medium, plated, and incubated at 37°C for 2h to settle fibroblasts. Thereafter, medium from the Petri dish was collected, cells were re-centrifuged at 250xg, and pelleted cells were re-suspended in medium and quantified by hemocytometer, using trypan blue exclusion to assure viability. Cells ($5x10^4$) were then plated in tissue culture dishes with media containing 2 mg/ml cytochalasin B (Sigma #C6637). At 24h and 48h post irradiation, treated cells were fixed with 3% paraformaldehyde and 10% sucrose (Sigma) and permeabilized with 100% methanol. Slides were stained with H&E and MN scoring was carried out at a magnification of 40X oil. Frequency of MN was determined in binucleate cells. MN were defined according to published criteria (12) as round structures of size between 1/16 to 1/3 of the mean diameter of main nuclei, staining at a similar intensity to the main nuclei and separated by cytoplasm from both nuclei. For each sample, approximately ~500 binucleate cells were scored.

Radiotherapy of prostate cancer patients undergoing IVIM DW-MRI studies: Patients were early retrieves from an IRB-approved randomized phase II study NCT02570919 treated at the Champalimaud Center in Lisbon, Portugal, which compared treatment with 45Gy in five consecutive 9Gy sessions versus a single dose of 24Gy, as described (13). Fusion CT/MRI simulation images were used for treatment planning. Prostate motion tracking during treatment was employed via use of electromagnetic beacon transponders temporarily placed endo-urethral catheter, prostate motion mitigation was achieve through the use of an endorectal balloon, and anatomical matching was assured via cone-beam CT immediately before treatment delivery using fast flattening-filter-free beam, Volumetric Arc (VMAT) technology.

Radiotherapy of oligometastatic bone lesions in patients undergoing IVIM DW-MRI studies: Patients were treated on an MSKCC IRB-approved prospective randomized study (MSKCC #10-154, NCT01223248). The trial was designed as a sub-study within a larger phase III randomized trial comparing two dosing schedules (24Gy SDRT versus a hypofractionated program of 3 fractions of 9Gy each) using image-guided radiation therapy in patients with metastatic bone cancer. Inclusion criteria were: (i) histologically-proven metastatic disease; patient deemed clinically appropriate for radiation treatment; (iii) life expectancy >6 months; age ≥ 18 years. Exclusion criteria

were: (i) inability to give informed consent; (ii) inability to comply with the protocol, (iii) contraindications to MRI; (iv) tumors involving visceral organs, brain or spinal cord; (v) platelet count <75,000/µl, hemoglobin level <9 g/dl, white blood count <3500/µl; (vi) metastases in the upper thoracic spine (to avoid MRI artifacts due to cardiac motion); (vii) lesions <1.5cm (to ensure robust measurements avoiding potential issues due to limited spatial resolution). Patients were treated according to standard clinical guidelines using a Varian megavoltage linear accelerator with on-board kilovoltage image-guidance capabilities, employing standard immobilization devices specific to the anatomical site treated.

1. Garcia-Barros M, Thin TH, Maj J, Cordon-Cardo C, Haimovitz-Friedman A, Fuks Z, and Kolesnick R. Impact of stromal sensitivity on radiation response of tumors implanted in SCID hosts revisited. *Cancer Res.* 2010;70(20):8179-86.
2. Horinouchi K, Erlich S, Perl DP, Ferlinz K, Bisgaier CL, Sandhoff K, Desnick RJ, Stewart CL, and Schuchman EH. Acid sphingomyelinase deficient mice: a model of types A and B Niemann-Pick disease. *Nat Genet.* 1995;10(3):288-93.
3. Platt J, Sodi S, Kelley M, Rockwell S, Bermudes D, Low KB, and Pawelek J. Antitumour effects of genetically engineered Salmonella in combination with radiation. *Eur J Cancer.* 2000;36(18):2397-402.
4. Kaplan DH, Shankaran V, Dighe AS, Stockert E, Aguet M, Old LJ, and Schreiber RD. Demonstration of an interferon gamma-dependent tumor surveillance system in immunocompetent mice. *Proc Natl Acad Sci U S A.* 1998;95(13):7556-61.
5. Thrall DE, Gillette EL, and Dewey WC. Effect of heat and ionizing radiation on normal and neoplastic tissue of the C3H mouse. *Radiat Res.* 1975;63(2):363-77.
6. Mahmood U, Alfieri AA, Thaler H, Cowburn D, and Koutcher JA. Radiation dose-dependent changes in tumor metabolism measured by 31P nuclear magnetic resonance spectroscopy. *Cancer Res.* 1994;54(18):4885-91.
7. Euhus DM, Hudd C, LaRegina MC, and Johnson FE. Tumor measurement in the nude mouse. *J Surg Oncol.* 1986;31(4):229-34.
8. Garcia-Barros M, Paris F, Cordon-Cardo C, Lyden D, Rafii S, Haimovitz-Friedman A, Fuks Z, and Kolesnick R. Tumor response to radiotherapy regulated by endothelial cell apoptosis. *Science.* 2003;300(5622):1155-9.
9. Yang W, Sheng H, Warner DS, and Paschen W. Transient global cerebral ischemia induces a massive increase in protein sumoylation. *J Cereb Blood Flow Metab.* 2008;28(2):269-79.
10. Mendez J, and Stillman B. Chromatin association of human origin recognition complex, cdc6, and minichromosome maintenance proteins during the cell cycle: assembly of prereplication complexes in late mitosis. *Mol Cell Biol.* 2000;20(22):8602-12.
11. Proia NK, Paszkiewicz GM, Nasca MA, Franke GE, and Pauly JL. Smoking and smokeless tobacco-associated human buccal cell mutations and their association with oral cancer--a review. *Cancer Epidemiol Biomarkers Prev.* 2006;15(6):1061-77.
12. Fenech M, and Morley AA. Measurement of micronuclei in lymphocytes. *Mutat Res.* 1985;147(1-2):29-36.
13. Arcangeli S, and Greco C. Hypofractionated radiotherapy for organ-confined prostate cancer: is less more? *Nat Rev Urol.* 2016;13(7):400-8.

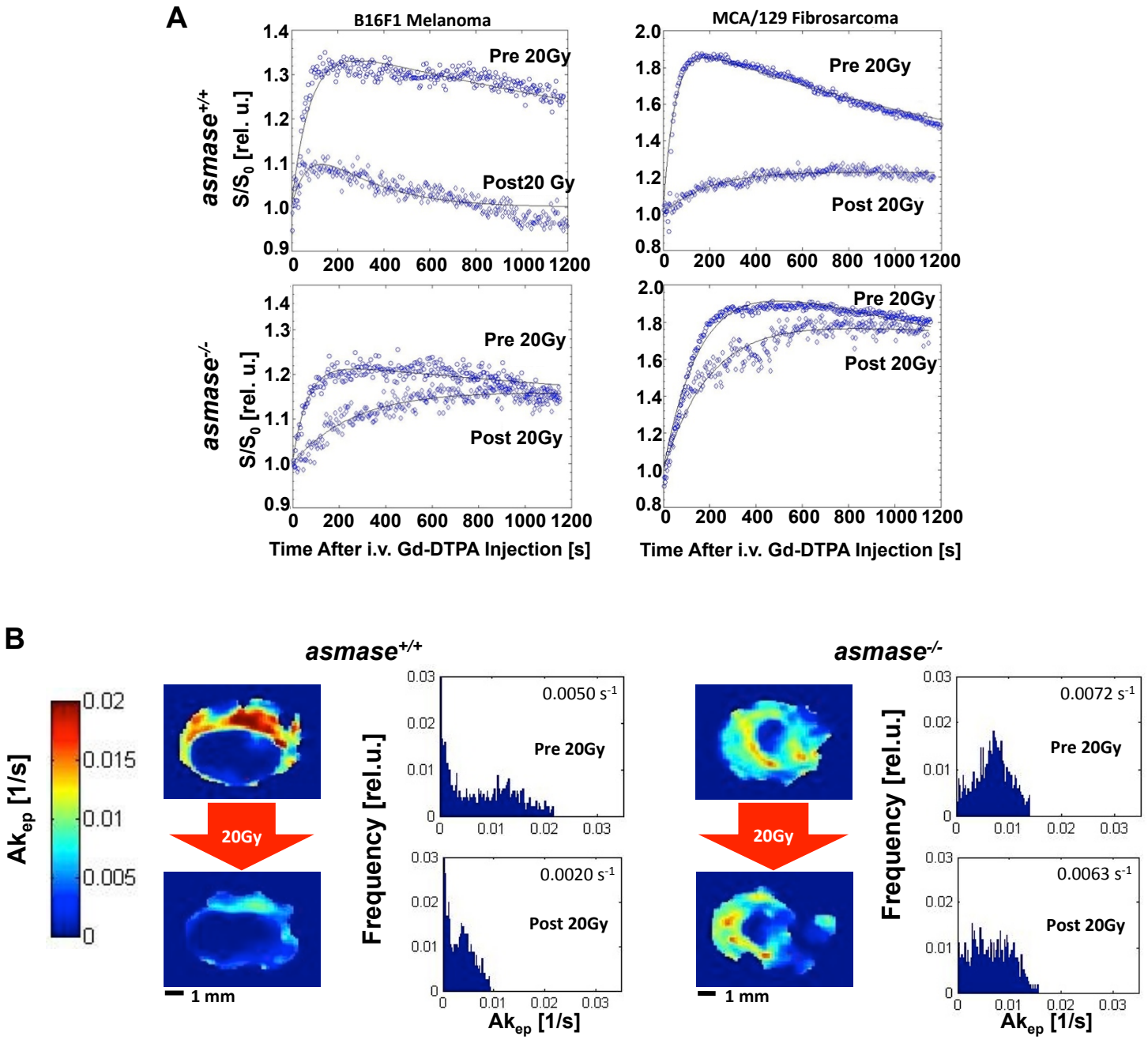

Supplementary Figure 1. (A) DCE-MRI time-signal curves of B16F1 melanoma and MCA/129 fibrosarcoma used for mathematical calculation of tumor Ak_{ep} values. A bolus injection of Gd-DTPA was delivered by tail vein into wild-type and *asmase*$^{-/-}$ tumor-bearing hosts before and at 30min after 20Gy SDRT. Time-signal data were obtained from the T1-weighted signal intensity of each individual voxel in 1mm DCE-MRI tumor slices for 20min after contrast injection and normalized to baseline signal. Data points were fitted according to a model developed by Hoffmann[76] based on the linear relationship between saturation recovery of the MR signal and concentration of Gd-DTPA in tissue. A two-compartment model is derived that consists of amplitude (A) reflecting degree of relative MR signal enhancement, and exchange rate (k_{ep}) characterizing velocity of MR signal increase. The Ak_{ep} value is analogous to the slope of time-dependent MR signal enhancement (the ascending portion of the curve), and is considered a quantitative surrogate of tumor perfusion. **(B)** DCE-MRI Ak_{ep} intensity maps and intensity histograms of reconstructed 1mm DCE-MRI MCA/129 fibrosarcoma tumor slices before and 30min after 20Gy SDRT. Tumors were implanted in wild-type and *asmase*$^{-/-}$ C57BL/6 hosts, and coded as in (A).

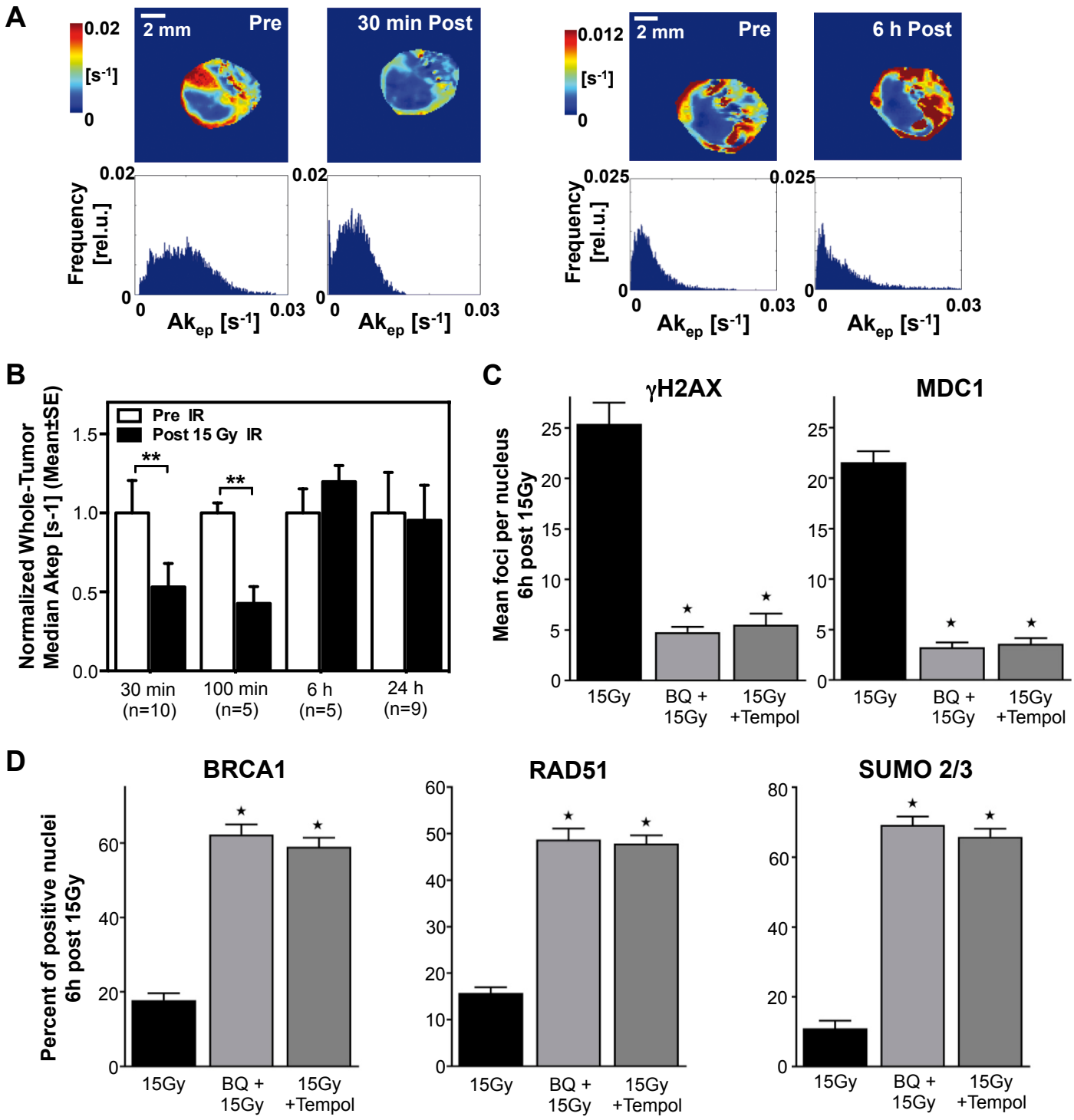

Supplementary Figure 2. (A) DCE-MRI studies of MCa mammary carcinoma tumors implanted in the foot of C3H/HeJ mice before and after 15Gy SDRT. Panels termed "Pre" show pre-SDRT color-coded Ak_{ep} intensity heat maps reconstructed from representative 1mm DCE-MRI slices (upper), and respective Ak_{ep} histograms (lower) quantified pixel-by-pixel across the slice and shown as median Ak_{ep} values. Panels to the right of "Pre" show equivalent Ak_{ep} intensity heat map and histograms at 30min and 6h post 15Gy SDRT, respectively. **(B)** Whole-tumor mount median Ak_{ep} values, normalized with respect to pre-irradiation values, as a function of time after 15Gy SDRT. **P<0.01 derived from paired, two-tailed t-test. Number of mice per group indicated in parentheses. **(C-D)** Tempol and BQ-123 (designated BQ) abrogates delayed γH2AX (left) and MDC1 (right) foci resolution **(C)** and restores BRCA1, RAD51 and SUMO2/3 loading into repair foci **(D)** after 15Gy SDRT. Data (C-D) represent mean±SEM collated from 3 independents experiments of 2 mice/group. *P<0.05

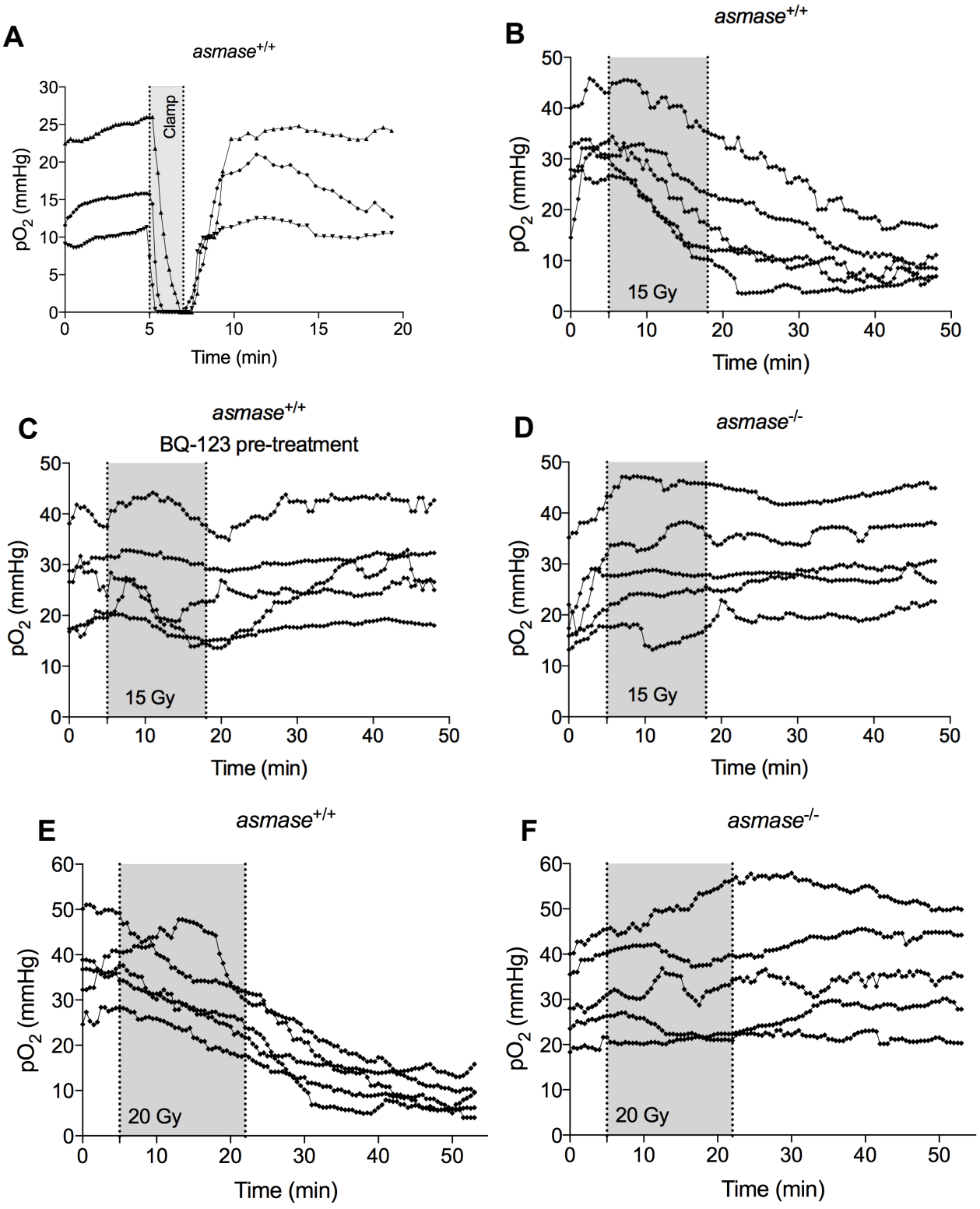

Supplementary Figure 3. (A) Each line represents one MCA/129 fibrosarcoma tumor implanted in the flank of a sv129/BL6 mouse. MCA/129 fibrosarcoma pO_2 is measured by OxyLite oximetry every 10-30sec in a constant tumor sub-volume in a mouse immobilized under isoflurane anesthesia before, during and after 2min percutaneous clamping of the major tumor-feeding blood vessels (n=3 mice). **(B to D)** pO_2 in MCA/129 fibrosarcoma measured before, during and after 15Gy SDRT in *asmase*$^{+/+}$ **(B),** *asmase*$^{+/+}$ mice pre-treated with BQ-123 **(C),** and in *asmase*$^{-/-}$ mice **(D)** (5 mice/group). Summary of these data is presented in Figure 1E. **(E-F)** pO_2 B16F1 melanoma measured before, during and after 20Gy SDRT in *asmase*$^{+/+}$ **(E)** and in *asmase*$^{-/-}$ mice **(F)** (5 mice/group).

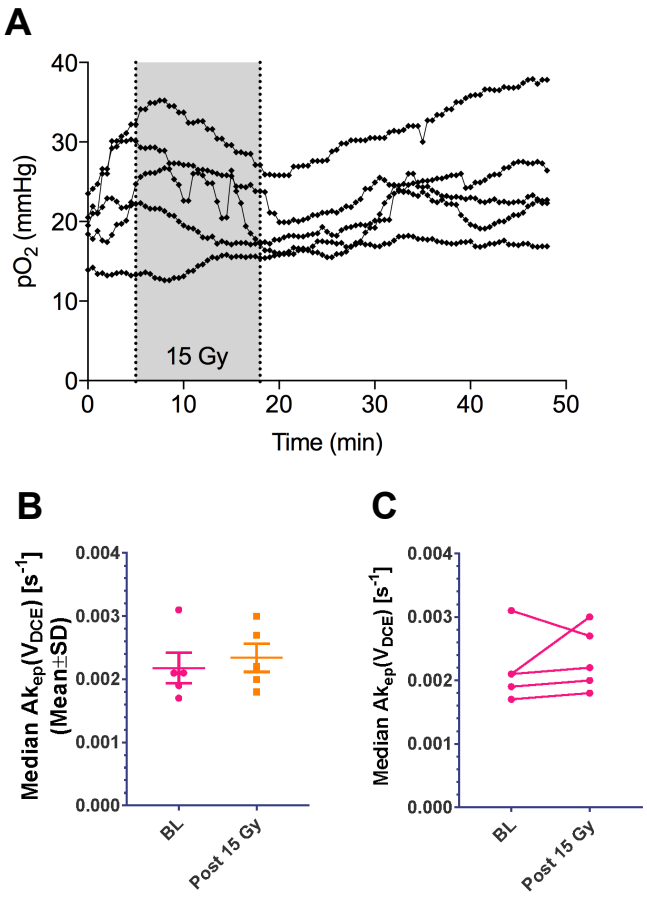

Supplementary Figure 4. (A) Time course of pO_2 measurement in vivo by OxyLite oximetry of normal subcutaneous tissue, sites of routine tumor implantation in the present studies. The OxyLite monitor probe was implanted in tumor non-bearing subcutaneous tissue of the flank and exposed to 15Gy SDRT. pO_2 was measured every 10-30sec in a constant tissue sub-volume of an mouse immobilized under isoflurane anesthesia before, during and after SDRT (n=5 mice). **(B)** Blood flow and perfusion DCE-MRI derived from DCE-MRI in a tumor non-bearing mouse thigh at baseline (BL) and after 15Gy SDRT (n=5 mice). **(C)** Paired pre- and post-SDRT (15Gy) Ak_{ep} blood flow and perfusion values of each mouse. No significant difference between pre- (BL baseline) and post- 15Gy SDRT.

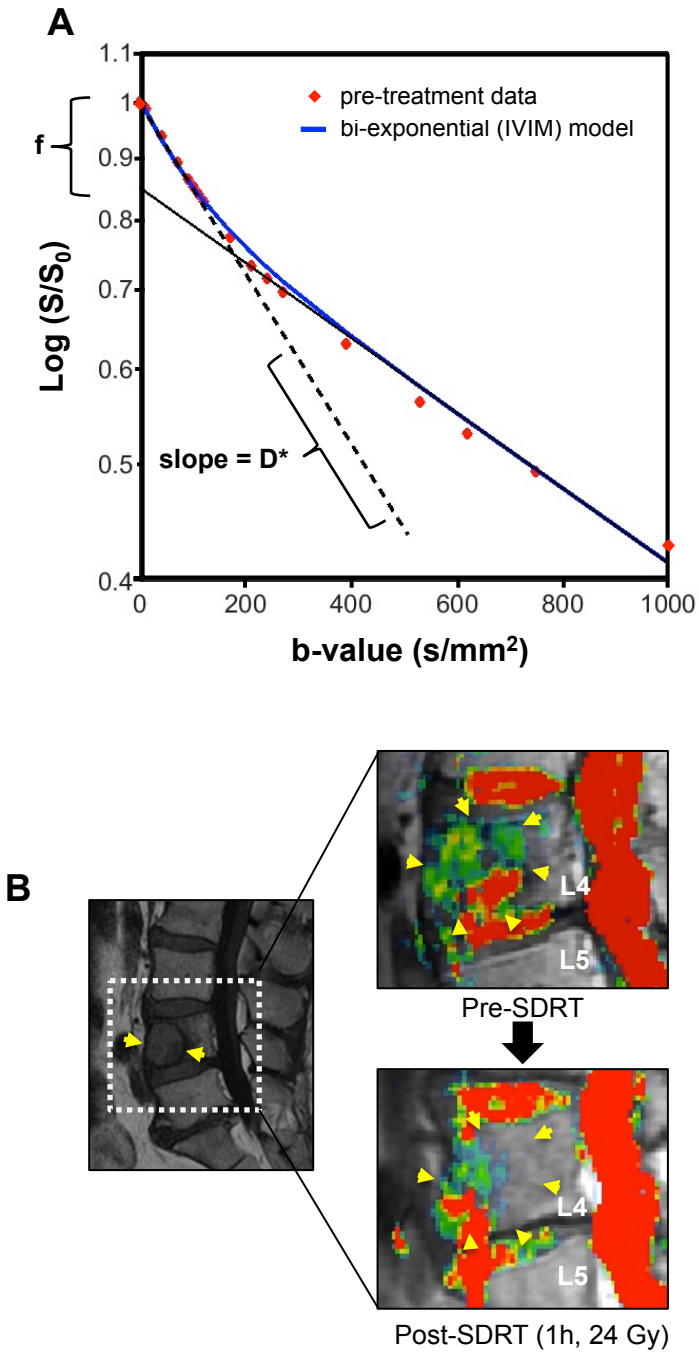

Supplementary Figure 5. (A) Dynamic IVIM DW-MRI obtains two values representing fraction of blood flow (f) and velocity (D*) in the microcirculation in patients. Shown is a schematic representation of the calculation of f and D* from the bi-exponential decay diffusion curve (black dashed lines). Filled squares represent an average curve of the whole tumor region, overlayed in blue with the bi-exponential fit. **(B)** An L4 spinal metastasis is delineated by yellow arrows in this T1-weighted sagittal MR image (left). f values are mapped pixel-by-pixel in color onto this image (right). Mean intensity of f declined rapidly following 24Gy SDRT in this patient.

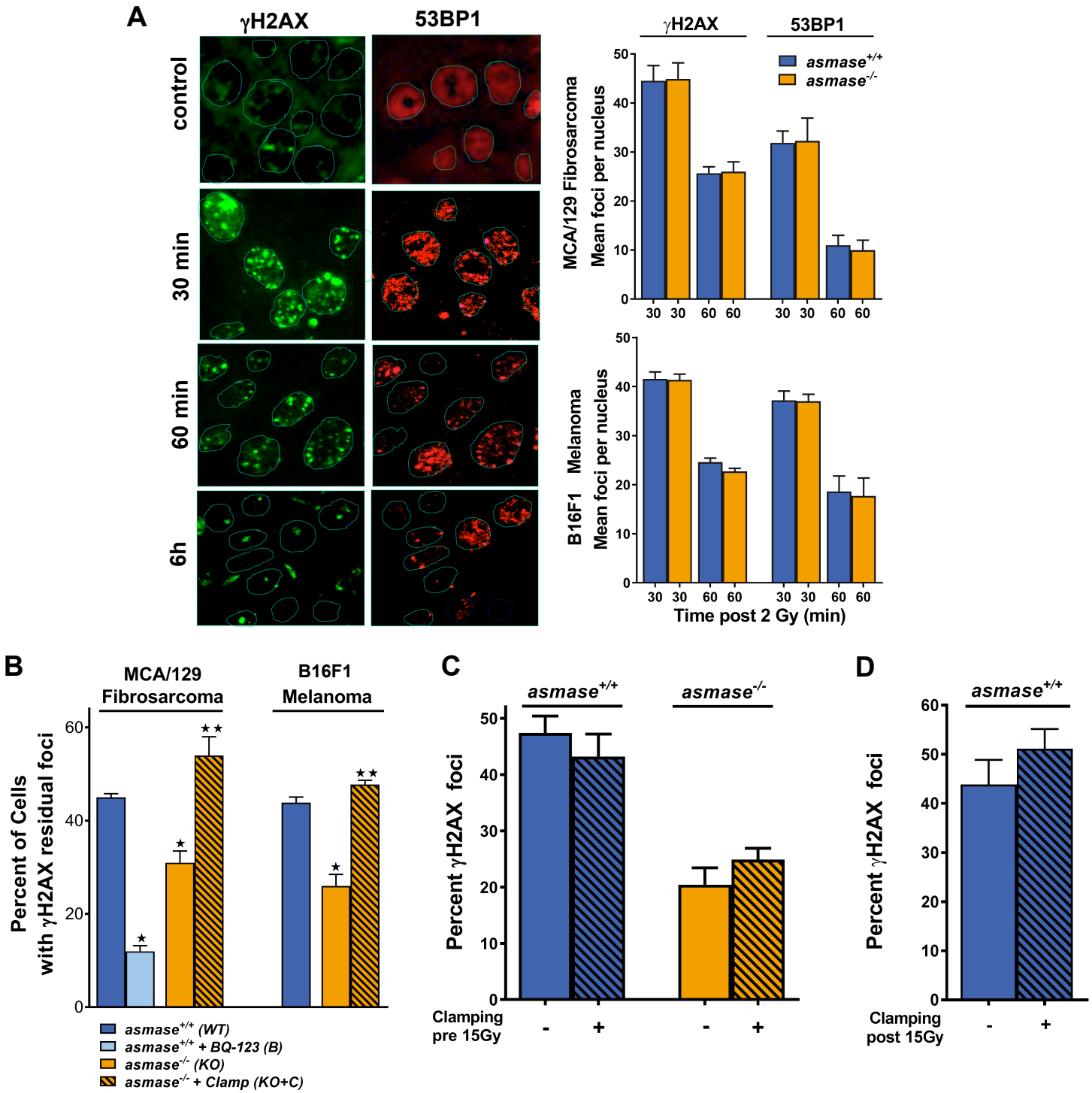

Supplementary Figure 6. (A) γH2AX and 53BP1 foci were detected by Axio Version microscopy in 3μm tumor sections following immunohistochemical staining with fluorescein-tagged antibodies against H2AX phospho-Ser139 (green) or 53BP1 (red). Typical staining of B16F1 melanoma foci in *asmase*$^{-/-}$ hosts (left) is quantified at 30 and 60min after 2Gy (right; data represent mean±SEM from 3-4 animals/point). **(B)** Impact of mechanical IR on γH2AX foci resolution in MCA/129 fibrosarcoma and B16F1 melanoma at 6h post 15Gy SDRT. Mechanical percutaneous clamping (designated C) of large tumor-feeding vessels was applied immediately post SDRT in *asmase*$^{-/-}$ (KO) hosts. BQ-123 (designated B) was injected i.p. at 30min prior to SDRT. *P<0.05 vs. WT, **P<0.001 vs. KO. **(C)** Control experiments examining impact of vascular clamping (2min) of B16 melanomas applied 10min before 15Gy SDRT failed to alter number of γH2AX foci in *asmase*$^{+/+}$ and *asmase*$^{-/-}$ hosts at 6h post radiation. **(D)** Control experiments examining impact of vascular clamping of B16F1 melanomas in *asmase*$^{+/+}$ hosts that display pathophysiologic vascular dysfunction had no additional effect on γH2AX foci at 6h after 15Gy SDRT.

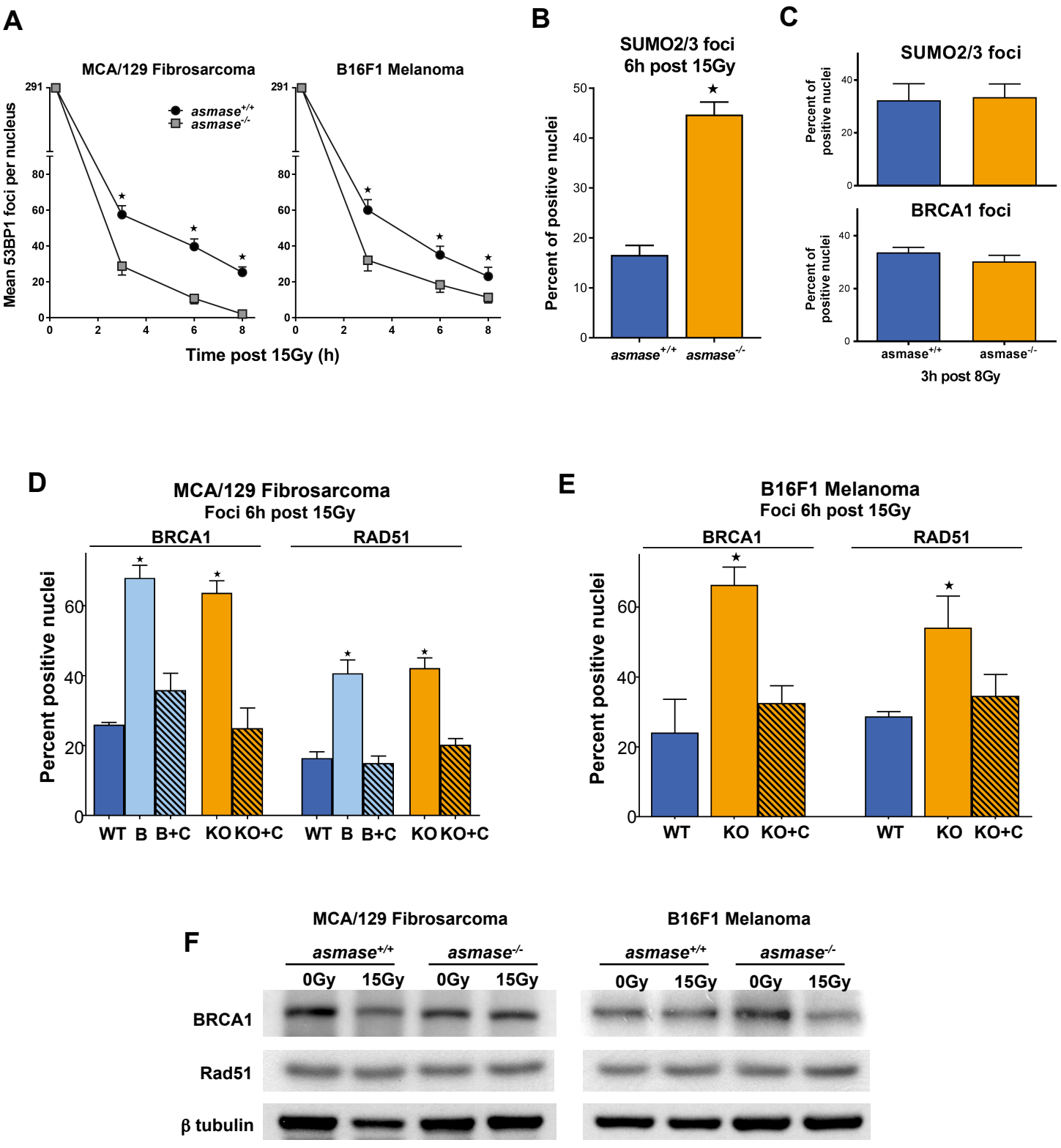

Supplementary Figure 7. (A) 53BP1 foci in MCA/129 fibrosarcomas (left) and B16F1 melanomas (right) were quantified at different times after 15Gy. *P<0.05 in *asmase*$^{+/+}$ vs. *asmase*$^{-/-}$ hosts. **(B)** Quantification of SUMO2/3 foci at 6h post 15Gy in MCA/129 fibrosarcomas. *P<0.05 in *asmase*$^{+/+}$ vs. *asmase*$^{-/-}$ hosts. **(C)** Quantification of SUMO2/3 (upper) and BRCA1 (lower) foci at 3h post 8Gy in HCT116 colon carcinomas. **(D-E)** Quantification of BRCA1 and RAD51 foci at 6h post 15Gy in MCA/129 fibrosarcomas (D) and B16F1 melanomas (E). Mechanical percutaneous clamping (designated C) of large tumor-feeding vessels was applied immediately post SDRT in *asmase*$^{-/-}$ (KO) hosts. BQ-123 (designated B). *P<0.05 vs. WT. Data represent mean±SEM. **(F)** Western blots showing BRCA1 and RAD51 protein levels were similar in tumors in *asmase*$^{+/+}$ and *asmase*$^{-/-}$ mice before and at 6h after 15Gy SDRT.

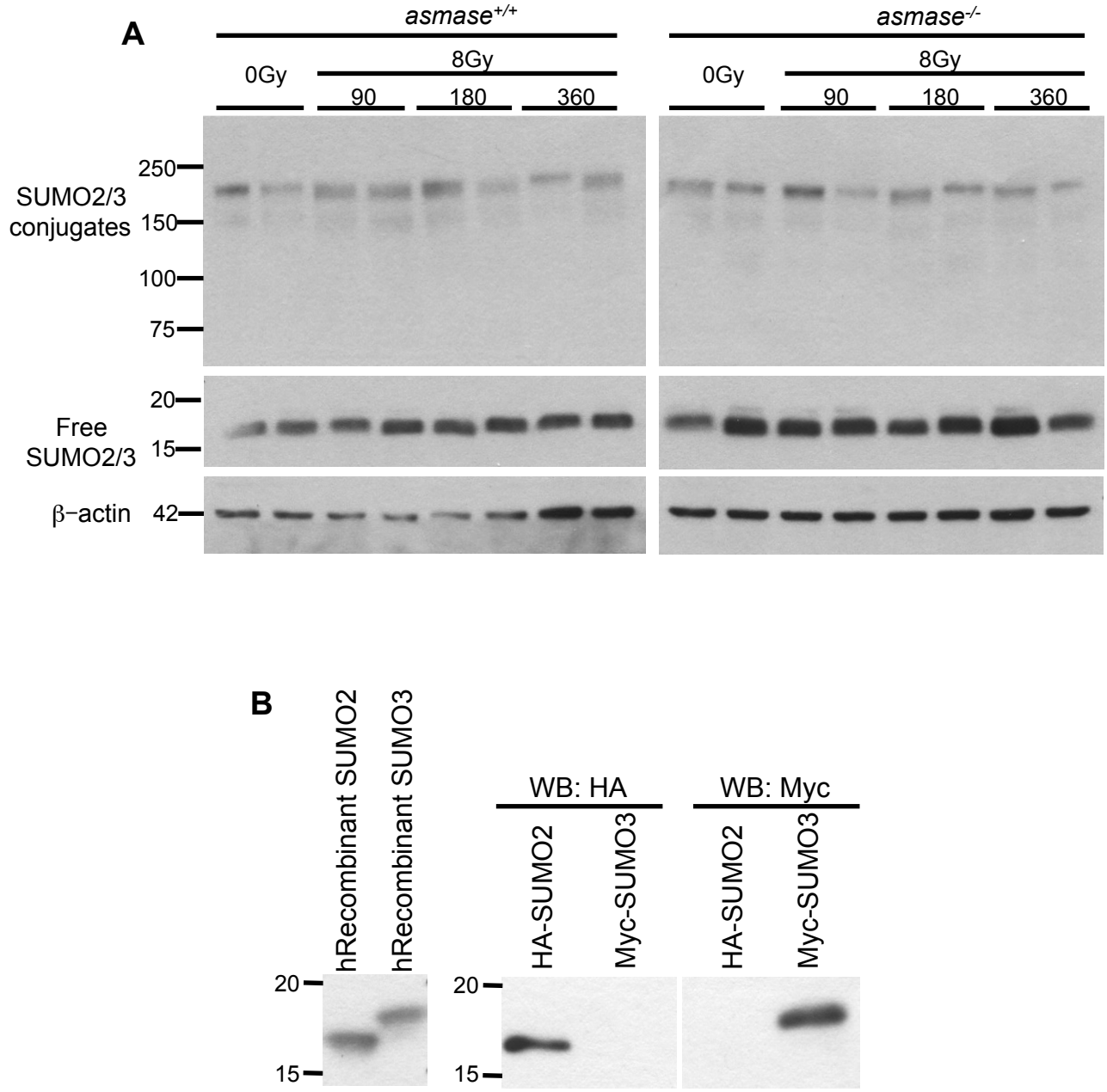

Supplementary Figure 8. (A) Representative western blots (WBs) from 1 of 3 similar experiments analyzing impact of 8Gy at 90-360min on SUMO2/3 conjugates (>75kDa) and free SUMO2/3 in whole cell extracts from MCA/129 fibrosarcomas in WT and KO hosts. β-actin serves as loading control. **(B)** WBs confirming SUMO2 and SUMO3 migration size. Left - Human recombinant protein (Novoprotein #C176 and #CE04 respectively) detected with rabbit polyclonal anti-SUMO2/3 Ab (Abcam #ab3742); Right – HCT116 cells transfected with HA-SUMO2 (Addgene plasmid #48967, gift from Guy Salvesen) and Myc-SUMO3 (Addgene plasmid #48964, gift from Guy Salvesen) plasmids from Addgene using Lipofectamine LTX DNA transfection kit following manufacturer's instructions. Cell lysates were analyzed at 48h post transfection using mouse monoclonal anti-HA Ab (Santa Cruz, #sc7392) and rabbit polyclonal anti-Myc Ab (Cell Signaling, #2278).

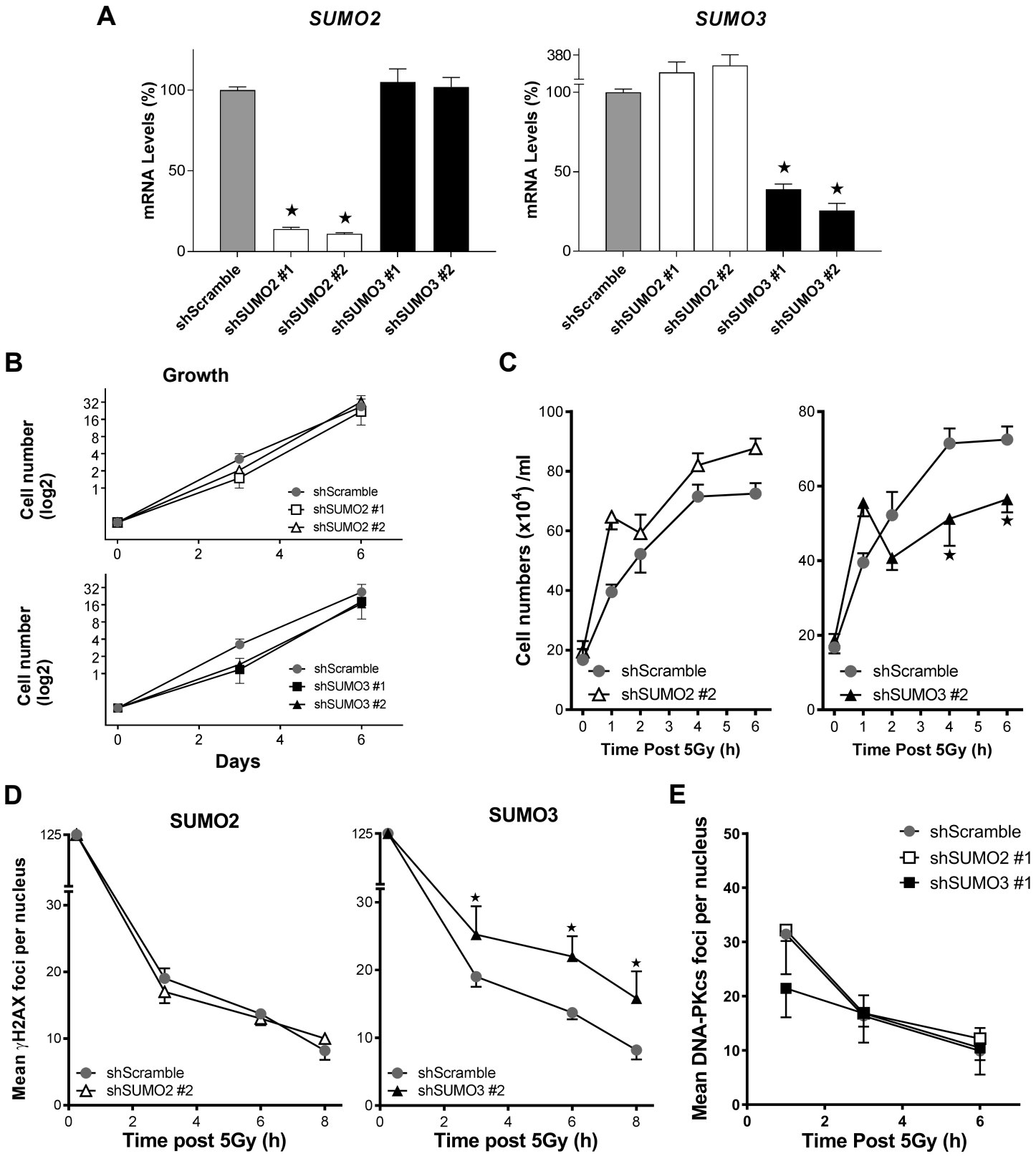

Supplementary Figure 9. (A) shRNA SUMO knockdown in HCT116 cells. Shown are RNA levels of 2 independent knockdown sets of cells for SUMO2 and SUMO3 measured by qPCR. Data represent mean±SEM from 1 of 4 similar experiments performed in triplicate. *P<0.05 vs. shScramble. **(B)** Impact of SUMO2 (upper) or SUMO3 (lower) knockdown on cell proliferation. Data represent mean ±SEM quantified by hemocytometer are collated from 2 experiments performed in triplicate. **(C-D)** Cell proliferation (C) and γH2AX focus kinetics (D) after 5Gy using set #2 of shRNA SUMO knockdown cells. *P<0.05 vs. shScramble. **(E)** Kinetics of DNA-PKcs focus resolution after 5Gy in shScramble, and shSUMO2 and shSUMO3 knockdown cells.

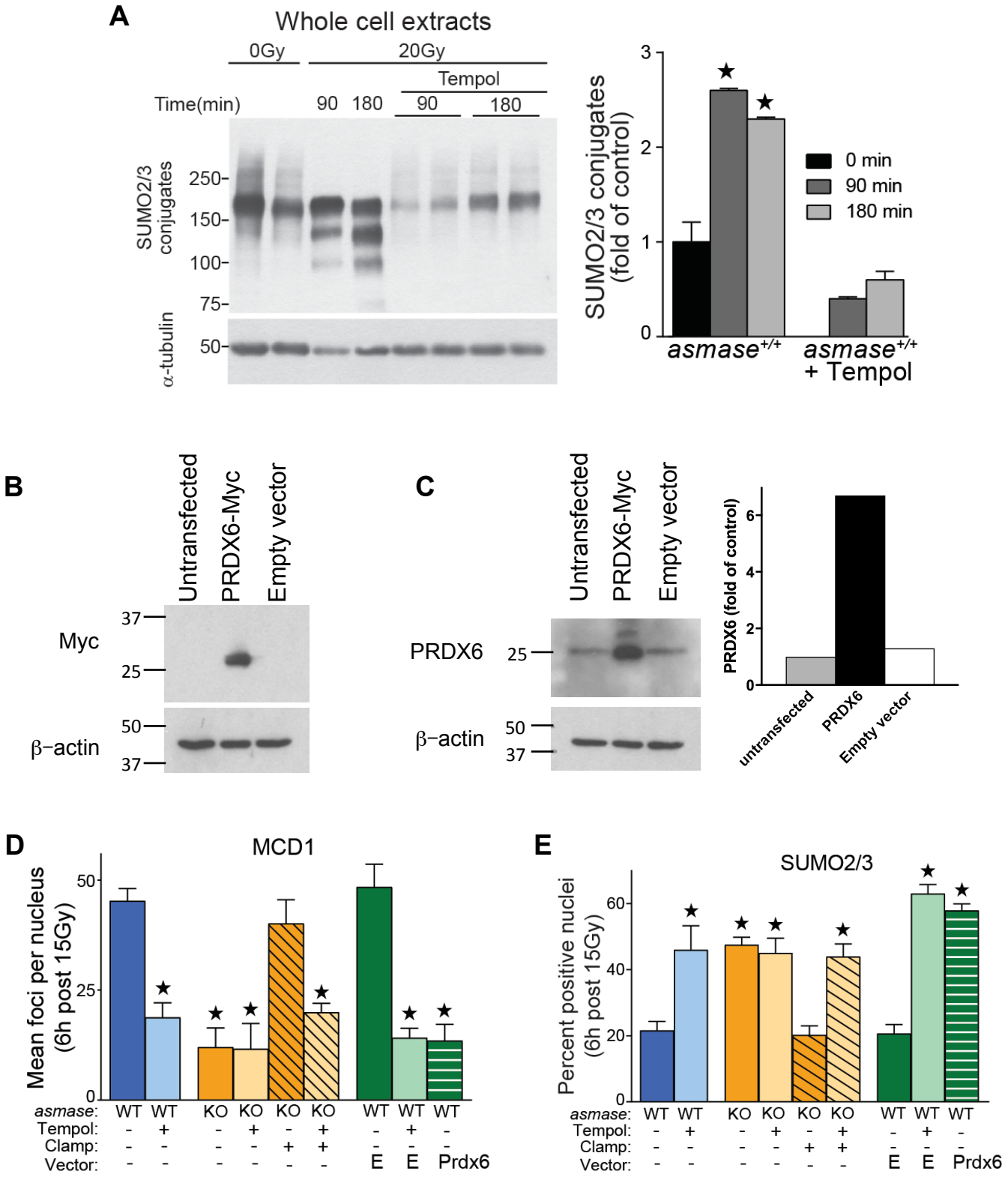

Supplementary Figure 10. (A) Western blot of whole cell extract of MCA/129 fibrosarcoma tumors using rabbit anti-SUMO2/3 antibody, quantified by densitometry relative to α-tubulin loading controls. Data represent mean±SEM from 3 independent experiments of 2 mice/group. **(B-C)** Western blot analysis of whole cell extracts of MCA/129 fibrosarcoma cells untransfected, transfected with PRDX6-Myc tag, or with empty vector, using **(B)** Myc antibody or **(C)** PRDX6 antibody (ab59543) quantified by densitometry relative to β-actin loading controls. **(D-E)** Overexpression of PRDX6 in MCA/129 fibrosarcomas mimics **(D)** tempol abrogation of delayed MDC1 focus resolution and **(E)** restores SUMO2/3 loading into repair foci. Negative control is an empty vector designated as E. Data represent mean±SEM from 2 independent experiments using 2 mice/group. *P<0.006 vs. WT **(D-E)**.

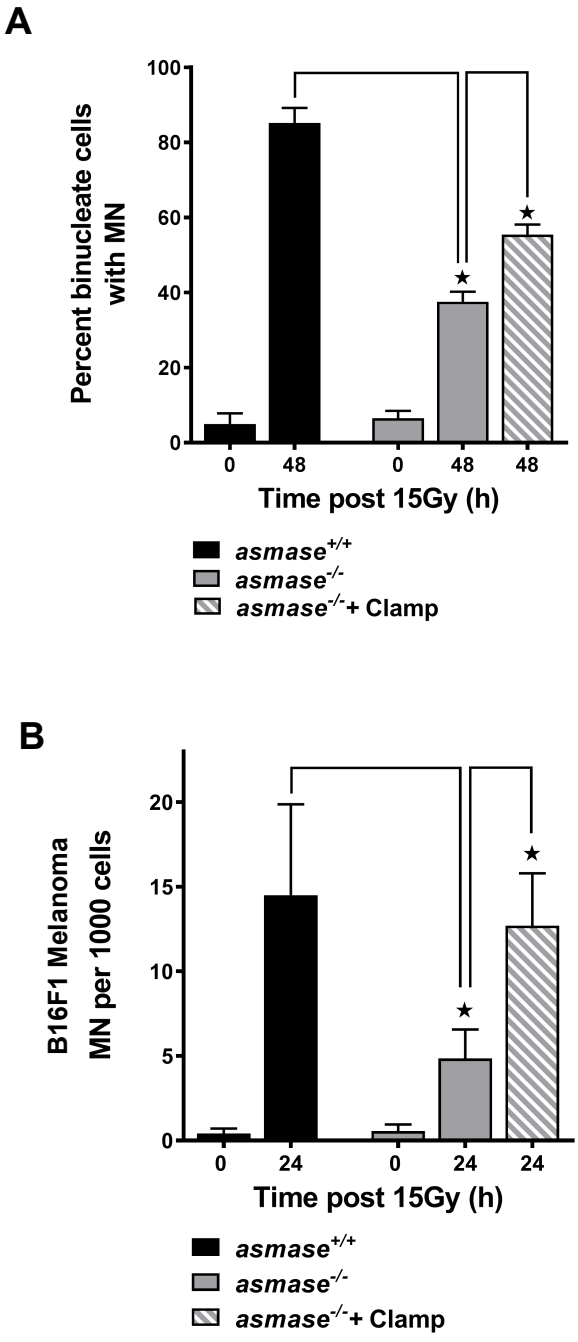

Supplementary Figure 11. (A) Micronuclei (MN) quantified by the ex vivo-cytochalasin B cytokinesis block method. MCA/129 fibrosarcoma tumors were irradiated (15Gy) in vivo, explanted ex vivo 1h later as single cell suspensions, treated with cytochalasin B, and scored for presence of binucleate MN at 24h (not shown) and 48h post irradiation. Data represent mean-incidence ±SEM of MN in 15Gy-treated MCA/129 fibrosarcomas counted in 80 cells/point from 2 experiments performed in triplicate. *P<0.05. **(B)** Data represent total MN quantification mean±SEM in vivo derived from 5μm H&E-stained B16F1 melanoma sections examining 2000 cells/tumor from 2 experiments performed in triplicate. *P<0.001 Bonferroni-Dunn.

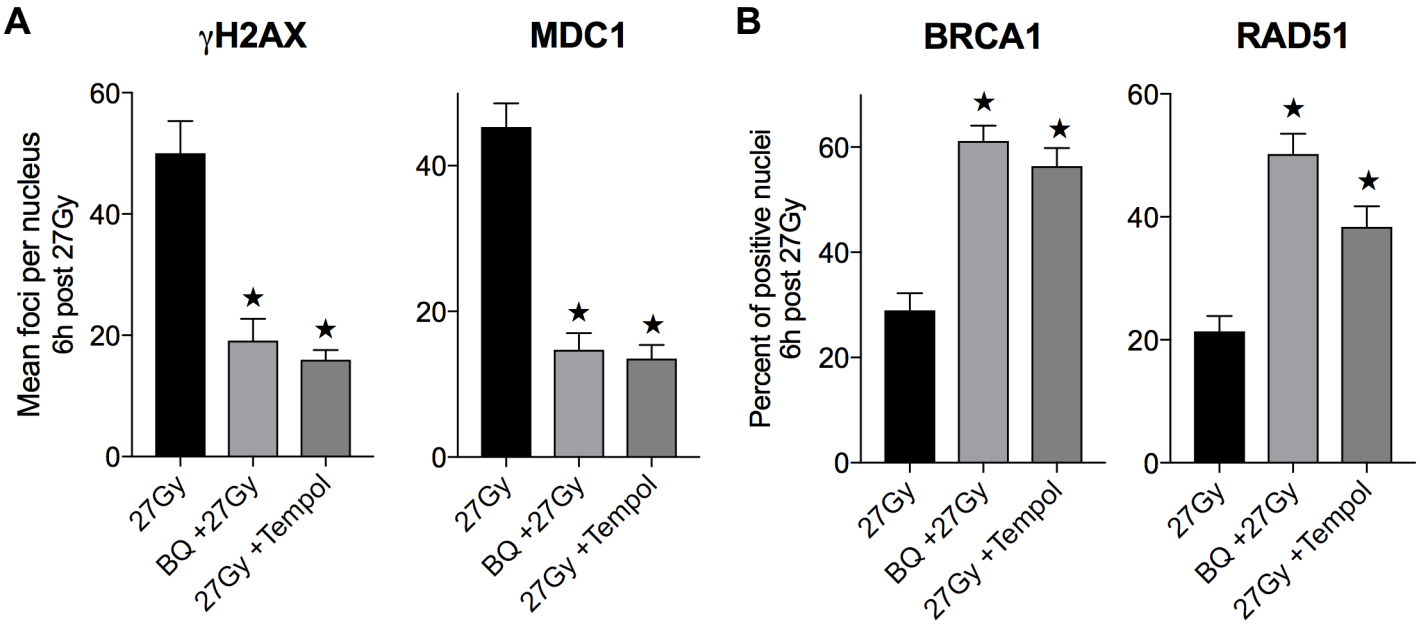

C	Tumor cured / total mice	γH2AX mean ± sem	MDC1 mean ± sem	BRCA1 mean ± sem	RAD51 mean ± sem
SDRT 27 Gy	8/17 (47%)	50 ±5.3	45.3 ±3.2	29 ±3.3	21.1 ±2.5
BQ-123 + 27Gy	1/10 (10%)	19.1 ±3.6	14.7 ±2.3	61.2 ±2.9	50.2 ±3.3
27Gy + Tempol	1/10 (10%)	16 ±1.5	13.6 ±1.9	56.4 ±3.4	38.4 ±3.4

Supplementary Figure 12. (A) Tempol and BQ-123 (designated BQ) abrogate delayed γH2AX (left) and MDC1 (right) focus resolution. **(B)** Tempol and BQ-123 restore BRCA1 (left) and RAD51 (right) loading into repair foci in SDRT-I/R (27Gy) MCA/129 fibrosarcoma tumors. *P<0.05 vs. 27Gy. Data represent mean±SEM from 2 independents experiments of 2 mice/group. **(C)** Correlation between tumor cure data, DSB markers (γH2AX & MDC1 foci) and DNA damage signaling markers (BRCA1 & RAD51 foci).

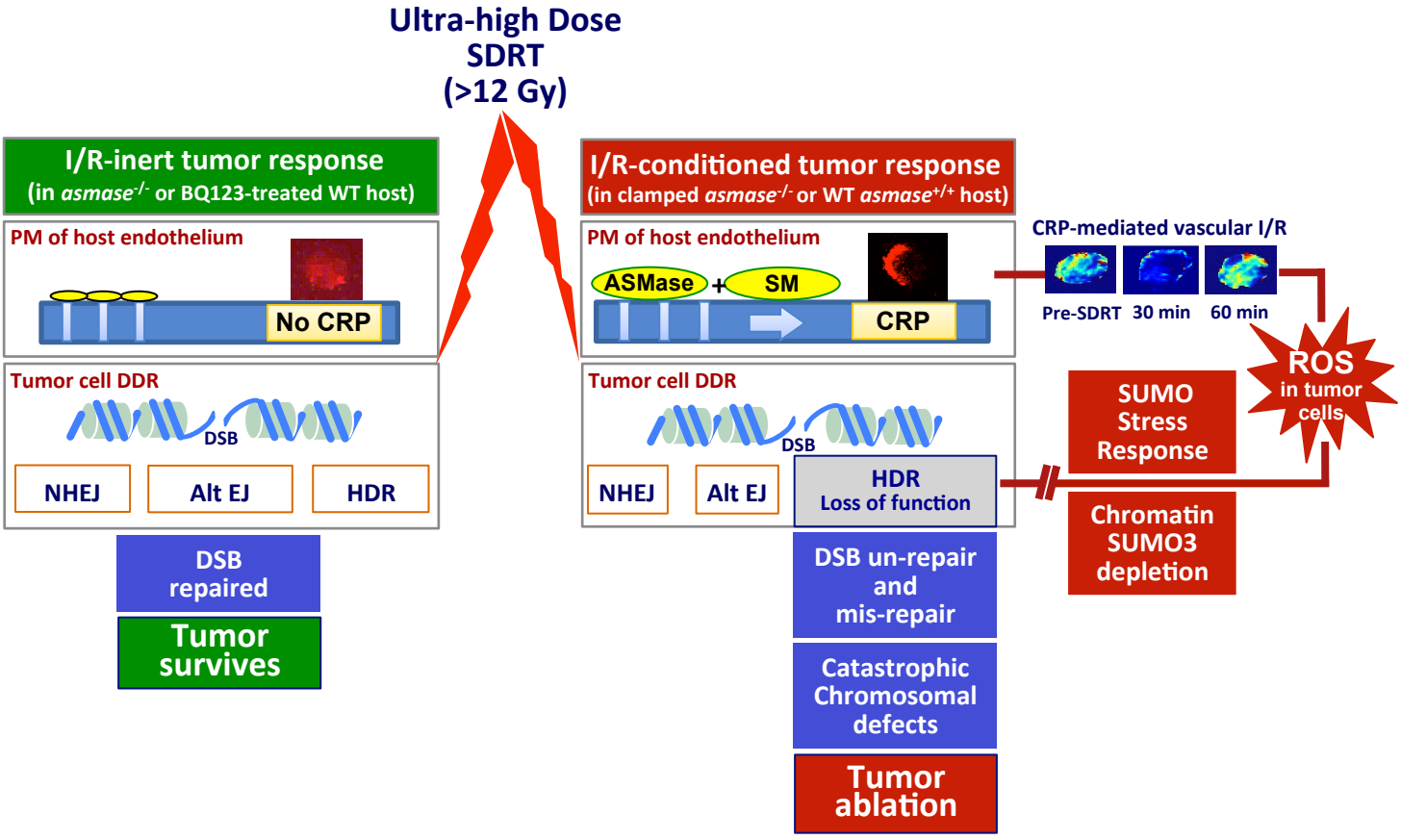

Supplementary Figure 13. The dual-target mechanism of tumor cure by SDRT: acid sphingomyelinase (ASMase)/ceramide-mediated ischemia reperfusion (I/R) injury to host-derived neo-angiogenic tumor microvasculature (SDRT-I/R) links with DNA damage repair (DDR) in parenchymal tumor cells to render synthetic tumor cell lethality. Right panels detail the pathophysiologic pathway of the SDRT-I/R-conditioned tumor response. SDRT exceeding a threshold dose of 10-12Gy activates ASMase translocation from cytosolic secretory lysosomes of tumor microvascular endothelium to the outer leaflet of the plasma membrane (PM), generating therein within minutes ceramide-rich platforms (CRPs), macrodomains that signal microvascular vasoconstriction. Resultant I/R injury to parenchymal tumor cells via acute hypoxia triggers therein generation of reactive oxygen species (ROS) and the adaptive SUMO Stress Response. The SUMO Stress Response is associated with specific depletion of chromatin-linked free SUMO3. Whereas SUMO3-ylation is indispensible for activation of homology-directed repair (HDR) of DSBs, HDR loss-of-function by SDRT-I/R yields DSB unrepair and misrepair, catastrophic chromosomal aberrations, and tumor clonogen demise. The left panels show that preventing I/R with the endothelin-1 inhibitor BQ-123 or by the use of *asmase*$^{-/-}$ mice as tumor hosts, abrogates CRP formation and SDRT-I/R, promoting full expression of the inherent tumor cell DDR, and tumor survival post SDRT. While these studies represent the initial conceptualization of this mechanism of SDRT tumor cure, substantive future investigation is required to elucidate more fully many aspects of this program.

Supplementary Table 1. Nadir values of f, D* and D derived from DW-MRI IVIM signals of tumor-bearing human prostate before and after radiation therapy

Treatment	**D** (10-3 mm2s-1)			**D*** (10-3 mm2s-1)			**f**		
	Pre-Tx	Post-Tx	% diff	Pre-Tx	Post-Tx	% diff	Pre-Tx	Post-Tx	% diff
24 Gy	0.64	0.53	-17.81	7.71	3.94	-48.9	0.19	0.086	-54.8
24 Gy	0.55	0.56	2.74	5.6	3.64	-33.21	0.23	0.073	-68.24
24 Gy	0.48	0.54	11.41	5.59	3.98	-28.79	0.37	0.17	-53.91
9 Gy	0.27	0.31	16.42	4.5	3.84	-14.58	0.087	0.094	8.05
9 Gy	0.57	0.48	-15.91	8.7	8.91	2.31	0.11	0.18	63.64

Supplementary Table 1 Nadir values of f, D* and D derived from IVIM DW-MRI signals before and after exposure of human prostate cancer to 24Gy SDRT or the first of 5 fractions of 9Gy hypofractionated radiotherapy.

Supplementary Table 2. IVIM DW-MRI data before and after radiation therapy of human oligometastaic tumors treated with either 24GySDRT or 3x9Gy hypofractionated radiotherapy

	Baseline, before RT				Following 24 Gy or 9Gy fraction				Fold Changes (After RT/Before RT)			
	D	D*	f	fD*	D	D*	f	fD*	D	D*	f	fD*
24 Gy												
1	0.860	0.0233	0.227	0.00528	0.660	0.0166	0.100	0.00166	0.77	0.71	0.44	0.31
2	0.735	0.0252	0.092	0.00226	0.576	0.0156	0.016	0.00025	0.78	0.62	0.17	0.11
3	0.602	0.0180	0.148	0.00281	0.576	0.0144	0.126	0.00183	0.96	0.80	0.85	0.65
4	0.662	0.0174	0.139	0.00244	0.573	0.0058	0.116	0.00067	0.87	0.33	0.84	0.27
5	0.433	0.0064	0.103	0.00066	0.429	0.0057	0.095	0.00054	0.99	0.89	0.92	0.81
6	0.555	0.0080	0.287	0.00230	0.522	0.0070	0.128	0.00088	0.94	0.87	0.45	0.38
7	0.601	0.0091	0.178	0.00157	0.576	0.0049	0.124	0.00060	0.96	0.53	0.69	0.39
8	0.630	0.0111	0.086	0.00098	0.621	0.0103	0.081	0.00084	0.99	0.92	0.94	0.86
9	0.549	0.0111	0.045	0.00049	0.582	0.0069	0.043	0.00027	1.06	0.62	0.97	0.54
Mean	0.625	0.0144	0.145	0.00209	0.568	0.0097	0.092	0.00084	0.92	0.70	0.70	0.48
SD	0.121	0.0068	0.076	0.00146	0.064	0.0047	0.039	0.00056	0.10	0.19	0.28	0.25
9 Gy x 1												
1	0.542	0.0252	0.083	0.00208	0.533	0.0264	0.071	0.00197	0.98	1.05	0.86	0.95
2	0.501	0.0101	0.095	0.00077	0.467	0.0102	0.083	0.00077	0.93	1.01	0.88	1.00
3	0.453	0.0066	0.342	0.00220	0.446	0.0074	0.305	0.00198	0.98	1.12	0.89	0.90
4	0.364	0.0096	0.052	0.00048	0.380	0.0068	0.051	0.00032	1.04	0.71	0.98	0.67
5	0.521	0.0153	0.098	0.00144	0.412	0.0111	0.087	0.00099	0.79	0.73	0.89	0.69
6	0.532	0.0077	0.119	0.00098	0.289	0.0066	0.121	0.00065	0.54	0.86	1.01	0.66
Mean	0.485	0.0124	0.131	0.00133	0.421	0.0114	0.120	0.00111	0.88	0.91	0.92	0.81
SD	0.067	0.0070	0.105	0.00070	0.083	0.0076	0.094	0.00070	0.19	0.17	0.06	0.15
9 Gy x 3												
1	0.542	0.0252	0.083	0.00208	0.581	0.0178	0.112	0.00200	1.07	0.71	1.35	0.96
2	0.501	0.0101	0.095	0.00077	0.412	0.0078	0.069	0.00053	0.82	0.77	0.72	0.69
3	0.453	0.0066	0.342	0.00220	0.375	0.0059	0.322	0.00190	0.83	0.89	0.94	0.86
4	0.364	0.0096	0.052	0.00048	0.348	0.0082	0.048	0.00037	0.96	0.86	0.94	0.77
5	0.521	0.0153	0.098	0.00144								
6	0.532	0.0077	0.119	0.00098	0.676	0.0069	0.109	0.00077	1.27	0.90	0.91	0.78
Mean	0.485	0.0124	0.131	0.00133	0.478	0.0093	0.132	0.00111	0.99	0.82	0.97	0.81
SD	0.067	0.0070	0.105	0.00070	0.143	0.0048	0.109	0.00078	0.19	0.08	0.23	0.10